THE JOURNAL OF BIOLOGICAL CHEMISTRY VOL. 287, NO. 7, pp. 4590–4601, February 10, 2012

Deficiency of Cardiolipin Synthase Causes Abnormal Mitochondrial Function and Morphology in Germ Cells of *Caenorhabditis elegans*[*]

Received for publication, October 18, 2011, and in revised form, December 15, 2011 Published, JBC Papers in Press, December 15, 2011, DOI 10.1074/jbc.M111.314823

Taro Sakamoto[‡1], Takao Inoue[§¶‖], Yukae Otomo[‡], Nagaharu Yokomori[‡], Motoki Ohno[‡], Hiroyuki Arai[§‖], and Yasuhito Nakagawa[‡]

From the [‡]School of Pharmacy, Kitasato University, Tokyo 108-8641, the [§]Graduate School of Pharmaceutical Sciences, University of Tokyo, Tokyo 113-0033, the [¶]Division of Cellular and Gene Therapy Products, National Institute of Health Sciences, Tokyo 158-8501, and [‖]CREST, Japan Science and Technology Agency, Tokyo 102-0075, Japan

Background: Cardiolipin is required for maintaining optimal mitochondrial function.
Results: Cardiolipin depletion selectively obstructed proliferation, mitochondrial function, and morphology in germ cells.
Conclusion: The contribution of cardiolipin to mitochondrial function and morphology varies among the different cell types *in vivo*.
Significance: This provides a biological basis for understanding the different sensitivities of organelles to changes in the lipid environment.

Cardiolipin (CL) is a major membrane phospholipid specifically localized in mitochondria. At the cellular level, CL has been shown to have a role in mitochondrial energy production, mitochondrial membrane dynamics, and the triggering of apoptosis. However, the *in vivo* role of CL in multicellular organisms is largely unknown. In this study, by analyzing deletion mutants of a CL synthase gene (*crls-1*) in *Caenorhabditis elegans,* we demonstrated that CL depletion selectively caused abnormal mitochondrial function and morphology in germ cells but not in somatic cell types such as muscle cells. *crls-1* mutants reached adulthood but were sterile with reduced germ cell proliferation and impaired oogenesis. In the gonad of *crls-1* mutants, mitochondrial membrane potential was significantly decreased, and the structure of the mitochondrial cristae was disrupted. Contrary to the abnormalities in the gonad, somatic tissues in *crls-1* mutants appeared normal with respect to cell proliferation, mitochondrial function, and mitochondrial morphology. Increased susceptibility to CL depletion in germ cells was also observed in mutants of phosphatidylglycerophosphate synthase, an enzyme responsible for producing phosphatidylglycerol, a precursor phospholipid of CL. We propose that the contribution of CL to mitochondrial function and morphology is different among the cell types in *C. elegans*.

Cardiolipin (CL)[2] is an anionic phospholipid with a unique diphosphatidylglycerol structure containing four acyl groups (1–3). In eukaryotic cells, CL localizes predominantly to the mitochondrial inner membrane, where it serves specific roles in mitochondrial structure and function. CL biosynthesis occurs via three enzymatic reactions, all catalyzed by enzymes present in the mitochondria (Fig. 1*A*) (4). The first step, catalyzed by phosphatidylglycerophosphate (PGP) synthase, is the synthesis of PGP from cytidine diphosphate-diacylglycerol (CDP-DAG) and glycerol 3-phosphate. PGP phosphatase dephosphorylates PGP to phosphatidylglycerol (PG). In the final step, CL synthase catalyzes the formation of CL from PG and CDP-DAG. These enzymes are highly conserved in eukaryotes (Figs. 1*A*, 2*B*, and 9*B*) (5).

So far, *in vitro* analysis has revealed that CL interacts with a number of mitochondrial proteins and is required for the optimal activity of several enzymes in the mitochondrial electron transport chain, including NADH dehydrogenase (complex I) (6), ubiquinol:cytochrome *c* reductase (complex III) (7–10), cytochrome *c* oxidase (complex IV) (11, 12), and ATP synthase (complex V) (13). Consistent with these observations, yeast CL synthase mutants (*crd1* mutants), in which CL is not detected, show instability of electron transport chain supercomplexes, perturbation of coupling, and reduced mitochondrial membrane potential, leading to a decrease in the oxidative phosphorylation rate (14–19). *crd1* mutants are viable under normal conditions; however, they show growth defects and mitochondrial DNA instability at high temperatures or under conditions of osmotic stress (14, 16). In contrast, knockdown of CL synthase in HeLa cells does not cause any defects in mitochondrial membrane potential, oxidative phosphorylation rate, or cell division under normal conditions (20, 21), although it is possible that residual CL may be sufficient to maintain normal mitochondrial function. In addition to the contribution of CL to mitochondrial oxidative phosphorylation, CL has also been shown to be involved in induction of apoptosis by interacting with pro-apoptotic proteins such as cytochrome *c* and tBid (22–24). As described above, the CL function has been analyzed

[*] This work was supported by Grant-in-aid for Scientific Research (C) 22590072 from the Japan Society for the Promotion of Science (to Y. N.) and by a Kitasato University research grant for young researchers (to T. S.).
[1] To whom correspondence should be addressed: School of Pharmacy, Kitasato University, 5-9-1 Shirokane, Minato-ku, Tokyo 108-8641, Japan. Tel.: 81-3-5791-6236; Fax.: 81-3-5791-6236; E-mail: sakamotot@pharm.kitasato-u.ac.jp.
[2] The abbreviations used are: CL, cardiolipin; CDP-DAG, cytidine diphosphate-diacylglycerol; $DiSC_3$, 3,3′-dipropylthiocarbocyanine iodide; PG, phosphatidylglycerol; PGP, phosphatidylglycerophosphate.

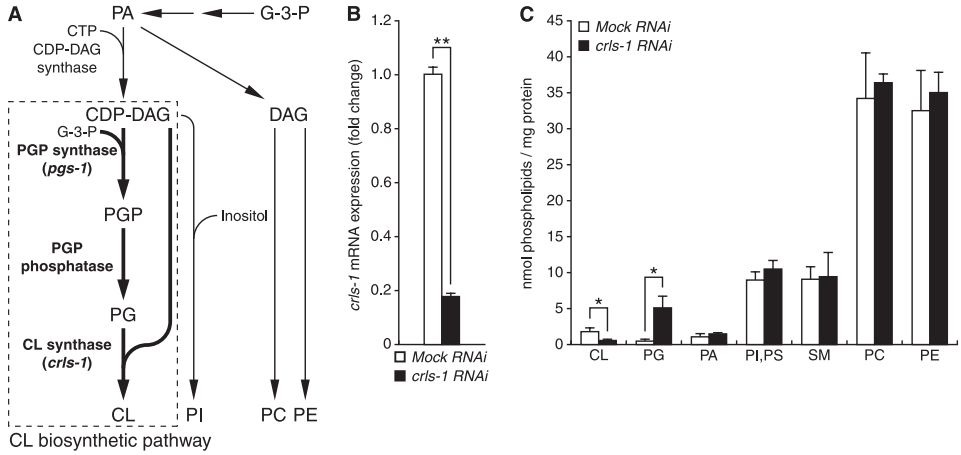

FIGURE 1. **CRLS-1 is the functional homologue of CL synthase in *C. elegans*.** *A*, schematic summary of phospholipid biosynthesis. Phospholipid biosynthesis branches into two pathways utilizing phosphatidic acid (*PA*) as an intermediate molecule. One branch of the pathway converts phosphatidic acid to DAG, which eventually produces phosphatidylcholine (*PC*) and phosphatidylethanolamine (*PE*). The other branch of the pathway converts phosphatidic acid to CDP-DAG, which is catalyzed by CDP-DAG synthase. CL biosynthetic pathway is *boxed* with *dashed lines*. Gene names in *parentheses* represent putative homologues in *C. elegans*. In this study, we used *crls-1* gene deletion mutants to reduce the content of CL, and *pgs-1* gene deletion mutants to reduce the content of both CL and PG. *B* and *C*, CL content is decreased in *crls-1*(*RNAi*) worms. Alterations and the expression of *crls-1* mRNA (*B*) and content of phospholipids (*C*) were examined in worms subjected to *crls-1* or mock RNAi. The expression of the *crls-1* gene was normalized to that of the *eft-3* gene and is represented as a fold change over the mock RNAi control. *G-3-P*, glycerol 3-phosphate; *PI,* phosphatidylinositol; *PS,* phosphatidylserine; *SM,* sphingomyelin. The data represent the mean ± S.D. **, $p < 0.01$; *, $p < 0.05$.

at the cellular level using yeast and mammalian cells. However, the *in vivo* role of CL in multicellular organisms is largely unknown.

Caenorhabditis elegans is a suitable model organism to investigate the effects of gene depletion on individual cells or tissues because it is anatomically simple and has invariant lineage. In this study, we analyzed *C. elegans* mutants lacking the CL synthase gene (*crls-1*) and found that CL is required for germ cell proliferation. The number of germ cells was reduced in *crls-1* mutants due to a reduction in the mitotic proliferation of germ cells. In the germ cells of *crls-1* mutants, the mitochondrial membrane potential was significantly decreased and the structure of the mitochondrial cristae was disrupted. However, somatic cells in *crls-1* mutants appeared normal with respect to cell proliferation, mitochondrial function, and mitochondrial morphology. These findings were confirmed by analysis of *C. elegans* mutants lacking a PGP synthase. This is the first study to show varying susceptibilities among different cell types to CL depletion *in vivo*.

EXPERIMENTAL PROCEDURES

General Methods and Strains—Maintenance and genetic manipulation of *C. elegans* were carried out as described previously (25). The Bristol strain N2 was used as the standard wild type strain. In addition, the following mutations, rearrangement, and transgenes were used: *pgs-1*(*tm2211*)*I*, *bli-3*(*e767*)*I*, *rrf-3*(*pk1426*)*II*, *crls-1*(*tm2542*)*III*, *crls-1*(*tm2575*)*III*, *qC1 dpy-19*(*e1259*) *glp-1*(*q339*)[*qIs26*]*III*, and *wIs51*[*scm*::*gfp*]. All strains were maintained at 20 °C. The deletion mutant strains *crls-1*(*tm2542*), *crls-1*(*tm2575*), and *pgs-1*(*tm2211*) were isolated as described previously (26). Each mutant was backcrossed seven times and was balanced with *qC1 dpy-19*(*e1259*) *glp-1*(*q339*)[*qIs26*] or *bli-3*(*e767*) for *crls-1*(*tm2542*) or *pgs-1*(*tm2211*), respectively.

Fluorescence and Nomarski Microscopy—Fluorescent images were obtained with an Axiovert 200 microscope (Carl Zeiss MicroImaging, Tokyo, Japan) equipped with a cooled AxioCam MRm CCD camera (Carl Zeiss MicroImaging) if not otherwise specified. Nomarski images were obtained with an IX71 microscope (Olympus, Tokyo, Japan) equipped with a cooled DS-5Mc CCD camera (Nikon, Tokyo, Japan).

Fixation and DAPI Staining—For gonad staining, young adult stage hermaphrodites were decapitated just below the pharyngeal bulb, allowing extrusion and extension of the gonad arms. The gonad was fixed with gonad fixative solution (3% formaldehyde, 75% methanol, and 6.2 mM K_2HPO_4 (pH 7.2)) for 10 min at room temperature. After washing twice with phosphate-buffered saline/Tween 20 (PBS-T, containing 0.1% Tween 20), the gonad was stained with 0.1 μg/ml DAPI in PBS-T for 10 min at room temperature. After washing twice with PBS-T, the gonad was mounted on a slide for observation.

Transgenic Rescue Analysis—DNA injection into the *C. elegans* germ line was carried out as described previously (59). A full-length cDNA of *crls-1* was amplified by PCR with the following primers: 5′-GGA AGT GGT ACC ATG ATA GTA ACA TCG ATG TT-3′ and 5′-GCG AAA ACG AGC TCT AAT TAA ATT TTT TTG ATG G-3′ (the underlined sequences are KpnI and SacI sites, respectively). The amplified fragments were cloned into the pPD49.78 and pPD49.83 heat-shock vectors (a gift from A. Fire) at the KpnI/SacI sites for pST1 and pST2, respectively. Two fragments containing a point mutation to change Asp-116 to Ala were amplified by PCR with the following primers: 5′-GGA AGT GGT ACC ATG ATA GTA ACA TCG ATG TT-3′ and 5′-GAG AAG TTT ATC AGC GAC AGG *AGC* AAG CAC G-3′; 5′-AAA TCA CTG CTT GGC TCC GTG CTT *GCT* CCT-3′ and 5′-GCG AAA ACG AGC TCT AAT TAA ATT TTT TTG ATG G-3′ (italicized nucleotides represent the Asp-to-Ala mutation). The two overlapping fragments were fused by PCR with following primers: 5′-GGA AGT GGT ACC ATG ATA GTA ACA TCG ATG TT-3′ and 5′-GCG AAA ACG AGC TCT AAT TAA ATT TTT

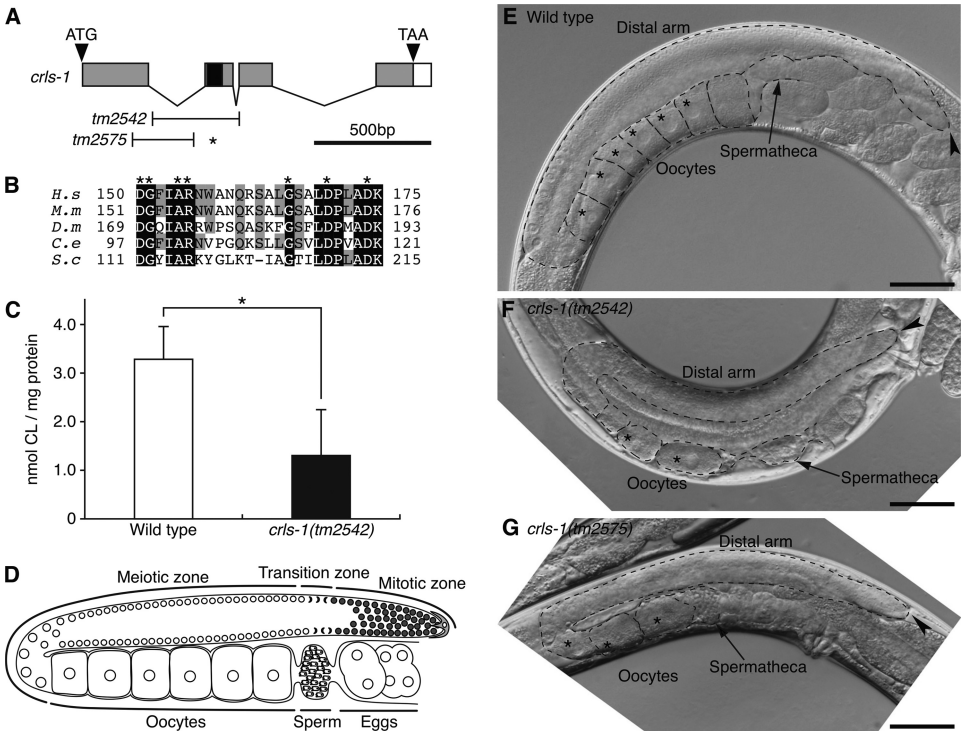

FIGURE 2. **Phenotypes of *crls-1* mutants.** *A*, genomic structure of *crls-1*. *Gray* and *white boxes* indicate exons and 3′-untranslated regions, respectively. The positions of the ATG start codon and TAA stop codon are shown. The *black box* indicates the DG*XX*AR*XXXXXXXX*G*XXX*D*XX*D sequence. *T-bars* below indicate the extent of deletion in *crls-1*(*tm2542*) and *crls-1*(*tm2575*). The deletion in *crls-1*(*tm2575*) causes a frameshift resulting in a premature stop codon (*asterisk*). *B,* multiple sequence alignment of the catalytic active motif of *C. elegans* CRLS-1 and homologous sequences in eukaryotes organized by ClustalW alignment. Residues identical in all five sequences are shaded in *black*, and residues identical in three or four proteins are shaded in *gray*. The accession numbers for the sequences used are as follows: (*H.s*) *Homo sapiens*, NP_061968; (*M.s*) *Mus musculus*, NP_001019556; (*D.m*) *D. melanogaster*, NP_733116; (*C.e*) *C. elegans*, NP_001022546; (*S.c*) *Saccharomyces cerevisiae*, NP_010139. *C,* content of CL was examined in wild type and *crls-1*(*tm2542*). The data represent the mean ± S.D. *, $p < 0.05$. *D*, schematic diagram of an adult hermaphrodite gonad. *E–G*, Nomarski images of the adult hermaphrodite gonads of wild type (*E*), *crls-1*(*tm2542*) (*F*), and *crls-1*(*tm2575*) (*G*) are shown. The gonads are outlined with the *dashed lines*. *Asterisks* indicate the germ nuclei at the diakinesis stage during oogenesis. *Arrowheads* indicate the distal end of each gonad. *Scale bars,* 50 mm.

TABLE 1

Viability and fertility of *crls-1* mutants

Adult hermaphrodites of the *crls-1* heterozygote were allowed to lay eggs for overnight at 20 °C, and the F1 progeny were scored for embryonic lethality and brood size. The brood sizes were determined by placing individual worms on seeded plates and allowing self-fertilization at the indicated temperature. The P0 worms were then transferred to a fresh plate at 24-h intervals for the next 4 days. The total F1 progenies on the plates were counted. Genotype of the animals were examined by genomic PCR. The data represent the mean ± S.D.

Genotype	Embryonic lethal	*n*	Brood size	*n*
	%			
Wild type	0	>500	320.94 ±39.39	63
crls-1(*tm2542*)	0	450	6.12 ±2.71	24
crls-1(*tm2575*)	0	435	3.76 ±2.43	21

TTG ATG G-3′. The amplified fragments, forming a full-length *crls-1*^{D116A} cDNA, were cloned into pPD49.78 and pPD49.83 at the KpnI/SacI sites for pST3 and pST4, respectively. The array *Ex*[*hsp*::*crls-1*] contained the plasmids pST1 (*hsp16-41*::*crls-1*), pST2 (*hsp16-2*::*crls-1*), and pRF4[*rol-6*(*su1006*)]. The array *Ex*[*hsp*::*crls-1*^{D116A}] contained the plasmids pST3 (*hsp16-41*::*crls-1*^{D116A}), pST4 (*hsp16-2*::*crls-1*^{D116A}), and pRF4. For the experiments of transgenic rescue of *crls-1* mutants, L1-staged hermaphrodites *crls-1*(*tm2542*), *crls-1*(*tm2542*);*Ex*[*hsp*::*crls-1*], and *crls-1*(*tm2542*); *Ex*[*hsp*::*crls-1*^{D116A}] were subjected to heat shock at 37 °C for 45 min. The heat-shocked hermaphrodites were transferred to new nematode growth medium plates individually and were incubated at 20 °C until they finished egg laying.

Analysis of Germ Cell Proliferation—The frequency of germ cell division was scored in the DAPI-stained extruded gonad (27). The boundary between the mitotic and transition zones was determined by the presence of the characteristic crescent-shaped germ nuclei, and the number of germ cells in the mitotic zone was counted. To calculate the frequency of germ cell divisions, the number of germ cells in the mitotic phase showing condensed chromatin or dividing nuclei was counted and then divided by the total number of germ cells in the mitotic zone.

Visualization of Seam Cell Nuclei—Seam cell nuclei were visualized using the *wIs51* transgene. *wIs51*[*scm*::*gfp*] expresses green fluorescent protein under a control of seam cell-specific promoters. Heterozygous *crls-1*(+/*tm2542*) or *pgs-1*(+/*tm2211*) worms, which carry a background transgenic insertion of *wIs51*, were generated. Gravid hermaphrodites were placed on nematode growth medium plates and incubated for 2 h to lay eggs. After removal of the parent hermaphrodites, the F1 progeny were incubated for 48 h. Young adult F1 hermaphrodites were mounted on a 4% agar pad and immobilized in 50 mM sodium azide. The number of seam cells on one lateral side was counted.

Determination of Mitochondrial Membrane Potential by DiSC$_3$—L4-staged hermaphrodites were placed on nematode growth medium plates containing 0.075, 0.15, or 0.3 μM of DiSC$_3$ (Sigma) and incubated for 24 h at 20 °C in the dark. Gonad arms were extruded and extended on a slide by decapi-

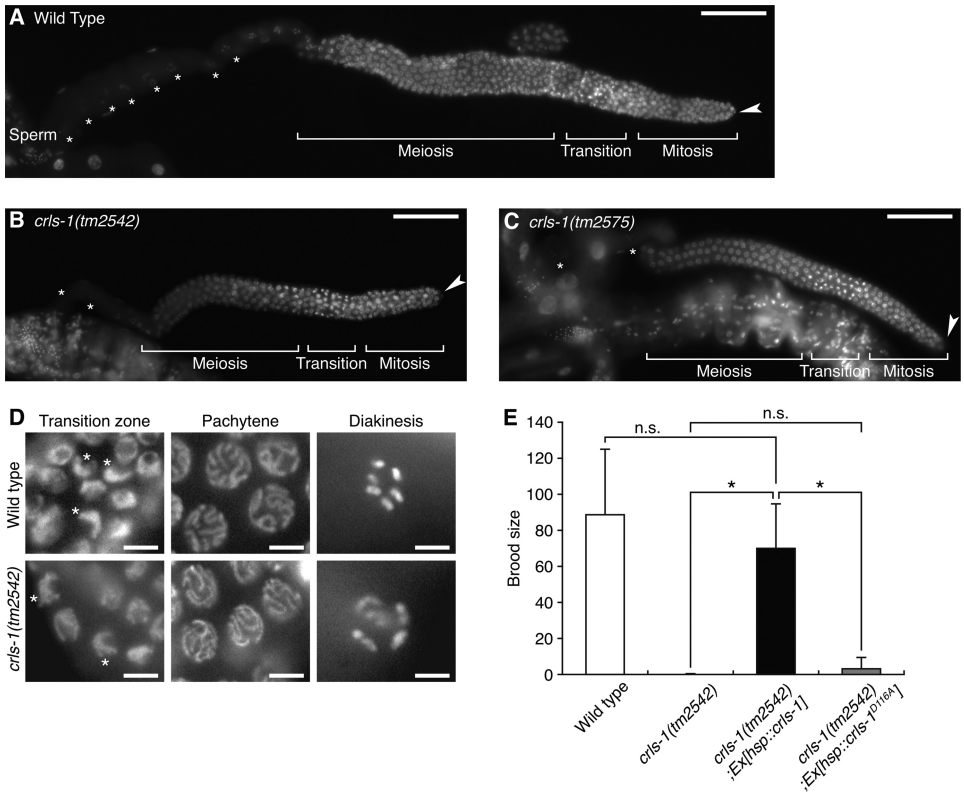

FIGURE 3. ***crls-1* is required for germ line development.** *A–C*, DAPI-stained images of adult hermaphrodite gonads of wild type (*A*), *crls-1*(*tm2542*) (*B*), and *crls-1*(*tm2575*) (*C*) are shown. The fluorescence signal from the sperm nuclei overlaps other portions of the specimen in *B* and *C*. *Asterisks* indicate the germ nuclei at the diakinesis stage during oogenesis. *Arrowheads* indicate the distal end of each gonad. *Scale bars,* 50 mm. *D,* DAPI-stained images of germ cell nuclei in adult hermaphrodite of the transition zone, pachytene stage, and diakinesis stage are shown. *Asterisks* indicate the typical crescent-shaped nuclei in the transition zone of germ cells. *Scale bars,* 5 mm. *E,* transgenic worms expressing the CRLS-1 or CRLS-1^{D116A} protein under the control of a heat shock promoter were produced as described under "Experimental Procedures." The brood sizes of wild type, *crls-1*(*tm2542*), and *crls-1*(*tm2542*) expressing exogenous CRLS-1 or CRLS-1^{D116A} were examined. Wild type and *crls-1*(*tm2542*) were derived from the same *crls-1*(+/*tm2542*) heterozygous mother. The data represent the mean ± S.D. *, $p < 0.05$; *n.s.*, not significant.

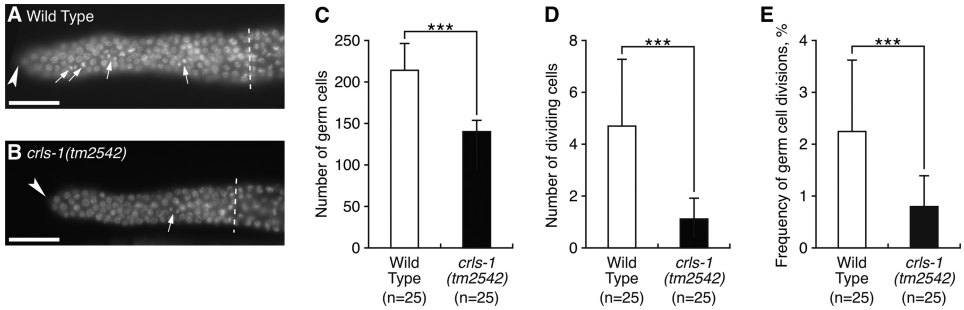

FIGURE 4. ***crls-1* is required for mitotic proliferation of germ cells.** *A* and *B*, DAPI-stained images of the mitotic zone in the adult hermaphrodite gonads of wild type (*A*) and *crls-1*(*tm2542*) (*B*) are shown. *Arrows* indicate nuclei in mitotic phase (M phase), showing condensed chromatin or dividing nuclei. *Arrowheads* indicate the distal end of each gonad. *Dashed lines* indicate the boundary between the mitotic and transition zones. *Scale bars,* 10 mm. *C–E*, quantitative analysis of germ cell mitosis in wild type and *crls-1*(*tm2542*). The data represent the mean ± S.D. ***, $p < 0.001$.

TABLE 2

Average number of vulval cells and seam cells in *crls-1* and *pgs-1* mutants

Genotype	No. of vulval cells	*n*	No. of seam cells	*n*
Wild type	22 ±0	16	16.03 ±0.44	90
crls-1(*tm2542*)[a]	22 ±0	8	16.09 ±0.67	40
pgs-1(*tm2211*)[b]	22 ±0	15	16.02 ±0.12	51

[a] *crls-1*(*tm2542*) homozygous mutants were derived from *crls-1*(*tm2542*)/*qC1* mother.

[b] *pgs-1*(*tm2211*) homozygous mutants were derived from *pgs-1*(*tm2211*)/*bli-3*(*e767*) mother. The data represent the mean ± S.D.

tation just below the pharyngeal bulb. To avoid rupture of the extruded gonad, the samples were sealed with a piece of PCR-slide seal. The intensity of $DiSC_3$ fluorescence was monitored on a BZ-8000 fluorescence microscope (Keyence, Tokyo, Japan) using a fixed exposure time and was quantified using ImageJ (National Institutes of Health, Bethesda). To determine the mean fluorescence values, the sum of the fluorescence values of the area corresponding to gonad or muscles was divided by the number of pixels.

Electron Microscopy—Transmission electron microscopy was performed by the Hanaichi Ultrastructure Research Institute Co. (Okazaki, Japan). Young adult hermaphrodites were fixed with 4% paraformaldehyde and 1% glutaraldehyde in 100 mM PBS for 1 h at 20 °C, followed by further fixation with 2% paraformaldehyde and 2% glutaraldehyde in 100 mM PBS for

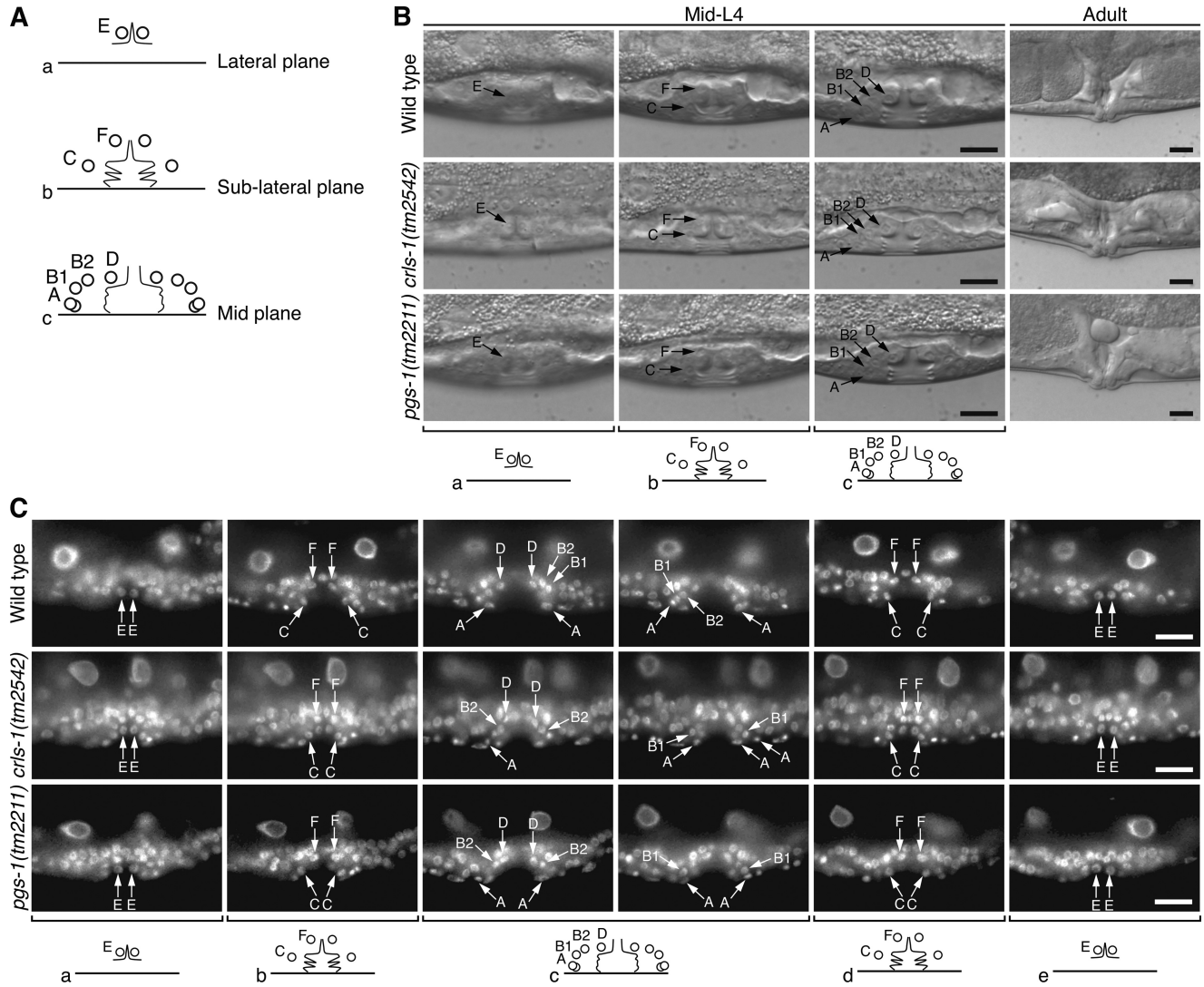

FIGURE 5. **Vulval cell divisions are normal in *crls-1* and *pgs-1* mutants.** *A*, schematic diagram of vulval cell positions in mid-L4 larva. *Circles, thin lines,* and *thick horizontal lines* indicate nuclei, cell boundaries, and the ventral cuticle, respectively. Anterior is *left* and dorsal is *top*. The letters *A*, *B1*, and *B2*, for example, correspond to the names of the vulval cells vulA, vulB1, and vulB2. *B* and *C*, positions of the vulval cells and the morphology of the mature vulva were observed by Nomarski microscopy (*B*) and DAPI staining (*C*). The *top*, *middle*, and *bottom panels* show wild type, *crls-1*(*tm2542*), and *pgs-1*(*tm2211*), respectively. Schematics corresponding to each focal plane are shown *below* the images. *Arrows* indicate the nuclei of each vulval cell lineage. *Scale bars,* 10 mm.

more than 24 h at 4 °C. The samples were post-fixed with 2% osmium tetroxide in 100 mM phosphate buffer for 4 h at 4 °C, followed by dehydration in an ethanol series, substitution with propylene oxide, and infiltration with Q651 resin (Mitsui Chemicals, Tokyo, Japan). Transverse sections were post-stained with uranyl acetate and lead citrate. The specimens were observed with a JEM-200EX electron microscope (JEOL, Tokyo, Japan).

Rhythmic Behavioral Analysis—Young adult hermaphrodites were placed in drops of PBS, and simple rhythmic thrashing swimming was measured. Swimming was scored as the number of seconds taken for 30 thrashes and calculated backward to the swimming rate. Each worm was scored twice.

RNAi—RNAi against the *crls-1* gene was performed by the feeding of double-stranded RNA as described previously (28). *Escherichia coli* strain HT115 (DE3) was transformed with the pPD129.36 L4440 DoubleT-7scriptII vector (a gift from A. Fire, Stanford University School of Medicine, Stanford, CA) containing the full-length cDNA region of *crls-1*. An empty pPD129.36 plasmid was used for a mock RNAi control. Single colonies of transformed *E. coli* were cultured in LB medium containing 100 μg/ml ampicillin overnight at 37 °C. The precultured *E. coli* was diluted 1:100 and incubated for 6 h at 37 °C. After that, *E. coli* was seeded on nematode growth medium plates containing 1 mM isopropyl β-D-thiogalactopyranoside and further incubated overnight at room temperature to induce the expression of double-stranded RNA. Late L4-staged hermaphrodites of *rrf-3* mutants were placed on the feeding RNAi plates and incubated overnight at 20 °C to lay eggs (29). The F1 progeny that were laid during this period were incubated for 48 h at 25 °C. Young adult F1 hermaphrodites were collected and used for biochemical analyses.

Total RNA Isolation and Quantitative Real Time PCR—Total RNA was extracted from young adult worms with Isogen (Nippongene, Toyama, Japan). cDNA was synthesized from the RNA using Moloney murine leukemia virus reverse transcrip-

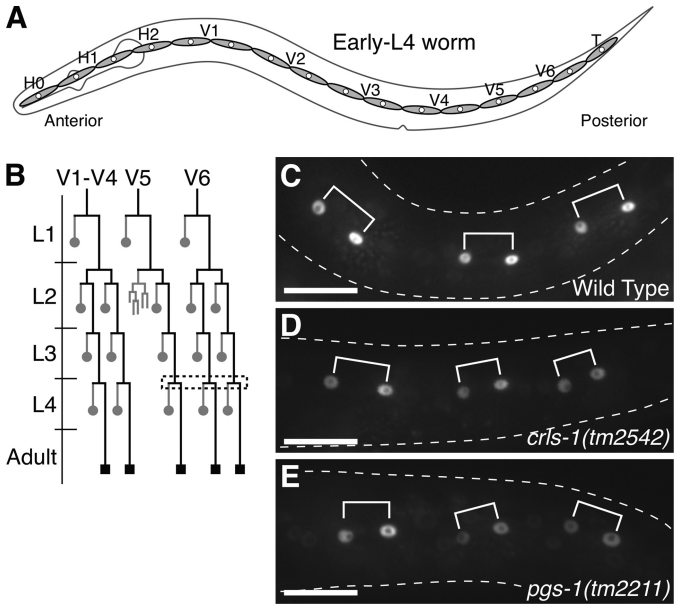

FIGURE 6. **Seam cell divisions are not affected in *crls-1* and *pgs-1* mutants.** *A*, schematic diagram of seam cells on each side in an early L4 larva. *B*, post-embryonic division pattern of V seam cells. The expression pattern of *scm*::*gfp*, which is specifically expressed in the nuclei of seam cells, is indicated by *black lines*. The *dashed box* marks the lineages observed in *C–E*. *Gray circles* represent anterior daughters that fuse with the epithelial syncytium, hyp7, and *black squares* denote seam cells. *C–E*, fluorescence images of *scm*::*gfp* just after the divisions at the L4 stage in wild type (*C*), *crls-1*(*tm2542*) (*D*), and *pgs-1*(*tm2211*) (*E*) are shown. The shapes of the worms are *outlined* with *dashed lines*. Three pairs of daughter cells are shown with *brackets*. *Scale bars,* 20 mm.

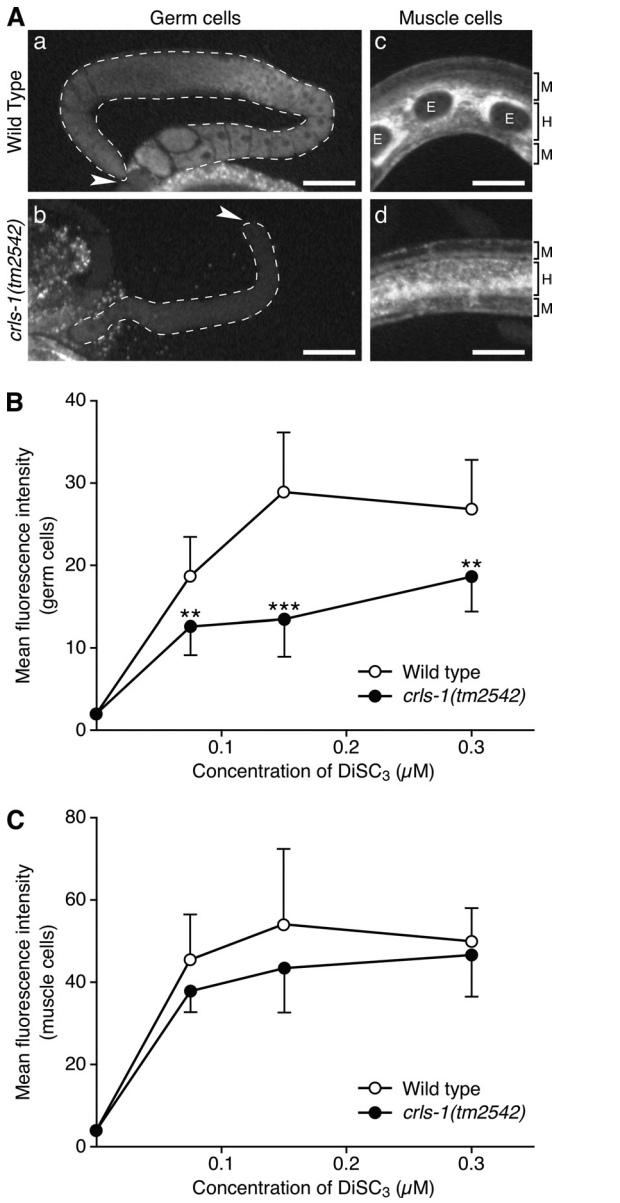

FIGURE 7. **Mitochondrial membrane potential is decreased in *crls-1* germ cells.** *A*, representative fluorescence images of germ cells (*panels a* and *b*) and muscle cells (*panels c* and *d*) in the wild type and *crls-1*(*tm2542*) stained with 0.15 μM $DiSC_3$ are shown. The gonads are outlined with the *dashed lines*. *Arrowheads* indicate the distal end of each gonad. *Brackets* on the *right-hand side* of the images (*panels c* and *d*) indicate the layers of muscle cells (*M*) and hypodermis (*H*). *E*, embryos. *Scale bars,* 50 mm. *B* and *C*, quantification of the fluorescence intensity of $DiSC_3$ in germ cells (*B*) and muscle cells (*C*) of wild type and *crls-1*(*tm2542*). The data represent the mean ± S.D. ***, $p < 0.001$; **, $p < 0.01$.

tase (Invitrogen). Quantitative real time PCR was performed using a CFX96 real time detection system with SsoFast EvaGreen Supermix (Bio-Rad). The sequences of the oligonucleotide primers used were as follows: 5′-CTC GGC TGT ATC ACA GGA TTC ACC A-3′ and 5′-ACG AGG AGG ATC ACA GTC TAG CGA-3′ for *crls-1*; 5′-GGC CGT CCC AGG AGA CAA CG-3′ and 5′-GAC CTG GGC GTG GAA GGT GC-3′ for *eft-3*. *eft-3* was amplified as an internal control, and *crls-1* gene expression was normalized against *eft-3* expression.

Lipid Analysis—Approximately 10,000 young adult worms were collected, and the total phospholipids were extracted using the method of Bligh and Dyer (30). Phospholipids were separated by one-dimensional thin layer chromatography on Silica Gel 60 TLC plates (Merck) in chloroform/methanol/acetic acid (65:25:13, v/v/v). Phospholipids were identified by comigration with known standards. The position of each spot was visualized by staining with 0.001% primuline in acetone/H_2O (4:1, v/v) under ultraviolet light. The area of silica gel corresponding to each phospholipid was scraped off and subjected to phosphorus quantification (31).

RESULTS

Identification of C. elegans CL Synthase crls-1—CL synthase catalyzes the formation of CL using PG and CDP-DAG as substrates (Fig. 1*A*) (1). A data base search of the complete *C. elegans* genome sequence revealed the presence of a single CL synthase homologue, F23H11.9, which we named *crls-1* (cardiolipin synthase homologue-1). The *crls-1* gene product, CRLS-1, consists of 246 amino acid residues and shows 45% identity with the human CL synthase. CRLS-1 has a CDP-alcohol phosphatidyltransferase motif that is highly conserved in the CRLS family proteins (32). In particular, the "DG*XX*-AR*XXXXXXXX*G*XXX*D*XXX*D" sequence, which is essential for the enzyme activity of CL synthase, is completely conserved within the phosphatidyltransferase motif of *C. elegans* CRLS-1 (Fig. 2*B*). To confirm that CRLS-1 contributes to CL synthesis in *C. elegans*, we determined the CL content in worms subjected to *crls-1* RNAi (Fig. 1, *B* and *C*). In *crls-1* RNAi worms, the expression of *crls-1* mRNA and the CL content were decreased to 18 and 39%, respectively, of those in mock RNAi worms (CL

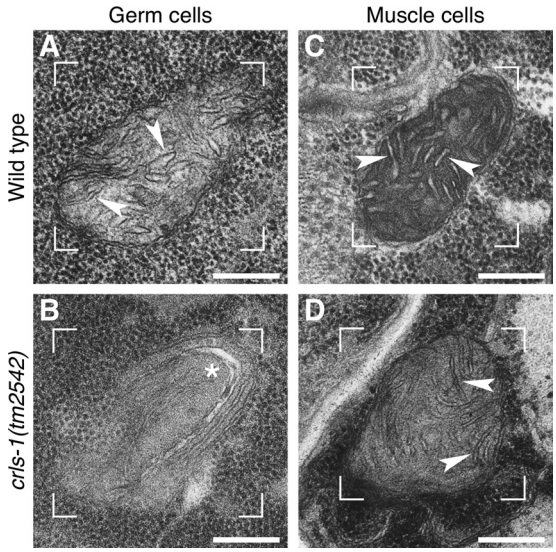

FIGURE 8. **Mitochondrial cristae structures are disrupted in *crls-1* germ cells.** Transmission electron micrographs of germ cells (*A* and *B*) and muscle cells (*C* and *D*) in wild type and *crls-1*(*tm2542*) are shown. In the mitochondrial matrix of *crls-1* germ cells, elongated inner membranes were located along the edge of the mitochondria, instead of the obvious cristae structures (*asterisk* in *B*). Representative mitochondria are enclosed by *brackets*. *Arrowheads* indicate the cristae structures. *Scale bars,* 200 nm.

content: 1.94 nmol/mg protein in mock RNAi worms *versus* 0.76 nmol/mg protein in *crls-1* RNAi worms). Concurrently, the content of PG, which is the precursor of CL, increased 8-fold in *crls-1* RNAi worms compared with mock RNAi worms (0.64 nmol/mg protein in mock RNAi worms *versus* 5.26 nmol/mg protein in *crls-1* RNAi worms). However, the amount of other phospholipids was not substantially affected in *crls-1* RNAi worms. These data indicate that CRLS-1 is a functional homologue of CL synthase in *C. elegans*.

crls-1 Is Required for Germ Cell Proliferation—To investigate the physiological role of CL *in vivo*, we examined the phenotypes of two different deletion alleles of *crls-1*; *tm2542* and *tm2575* (Fig. 2*A*). Both alleles lack the DG*XXX*AR*XXX*-*XXXXX*G*XXX*D*XXX*D sequence that is essential for the enzyme activity of CL synthase, suggesting that the products are functionless (Fig. 2*A*) (33). Consistent with the *crls-1* RNAi worms, the CL content was significantly decreased in *crls-1*(*tm2542*) (Fig. 2*C*). Both the *crls-1*(*tm2542*) and *crls-1*(*tm2575*) mutants were viable and reached adulthood; however, they showed extremely reduced brood size compared with the wild type (Table 1). In *C. elegans*, the gonadal arm of an adult hermaphrodite is U-shaped, with a distal arm containing a syncytium of germ line nuclei and a proximal arm containing oocytes and fertilized eggs (Fig. 2, *D* and *E*). Germ cells at the

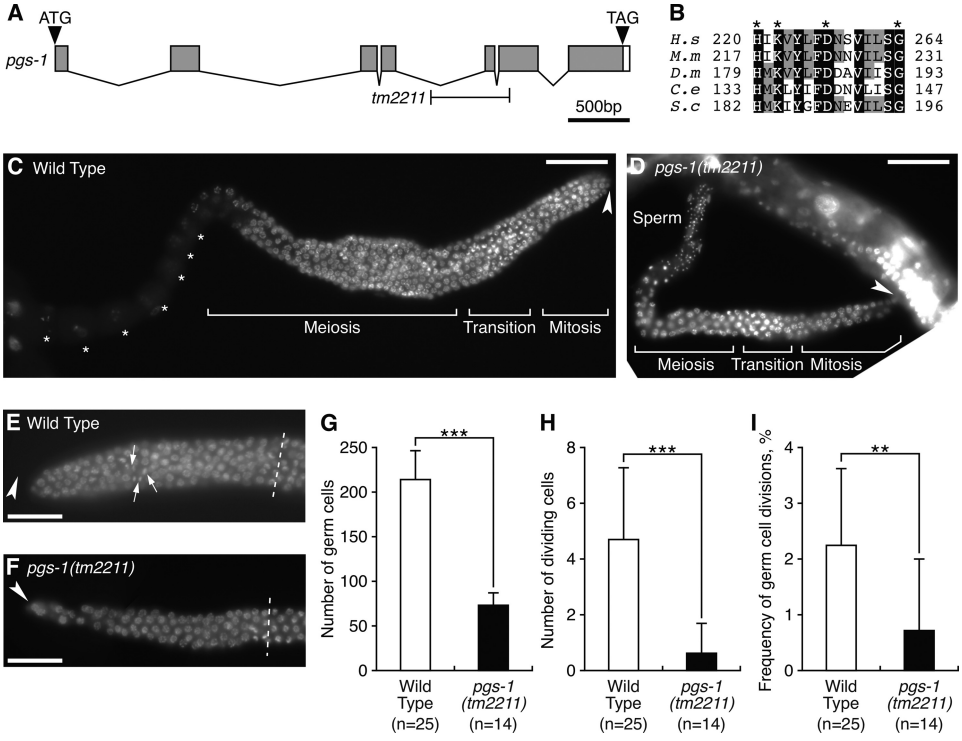

FIGURE 9. ***pgs-1* is required for the mitotic proliferation of germ cells.** *A*, genomic structure of *pgs-1*. *Gray* and *white boxes* indicate exons and 3′-untranslated regions, respectively. The positions of the ATG start codon and TGA stop codon are shown. *T-bars* below indicate the extent of deletion in *pgs-1*(*tm2211*). *B*, multiple sequence alignment of the catalytic active motif of *C. elegans* PGS-1 and homologous sequences in eukaryotes organized by ClustalW alignment. Residues identical in all five sequences are *shaded* in *black*, and residues identical in three or four proteins are *shaded* in *gray*. *Asterisks* indicate the H*X*K*XXXX*-D*XXXXX*G motif that is highly conserved in several hydrolases and phosphodiesterases. The accession numbers for the sequences used are as follows: (*H.s*) *H. sapiens*, NP_077733; (*M.s*) *M. musculus*, NP_598518; (*D.m*) *D. melanogaster*, NP_650751; (*C.e*) *C. elegans*, NP_490666; (*S.c*) *S. cerevisiae*, NP_009923. *C* and *D*, DAPI-stained images of adult hermaphrodite gonads of wild type (*C*) and *pgs-1*(*tm2211*) (*D*) are shown. The fluorescence signal from the sperm nuclei overlaps other portions of the specimen in *C*. *Asterisks* indicate the germ nuclei at the diakinesis stage during oogenesis. *Arrowheads* indicate the distal end of each gonad. *Scale bars*, 50 mm. *E* and *F*, DAPI-stained images of the mitotic zone in the adult hermaphrodite gonads of wild type (*E*) and *pgs-1*(*tm2211*) (*F*) are shown. *Arrows* indicate nuclei in M phase. *Arrowheads* indicate the distal end of each gonad. *Dashed lines* indicate the boundary between the mitotic and transition zones. *Scale bars,* 10 mm. *G–I*, quantitative analysis of germ cell mitosis in wild type and *pgs-1*(*tm2211*). The data represent the mean ± S.D. ***, $p < 0.001$; **, $p < 0.01$.

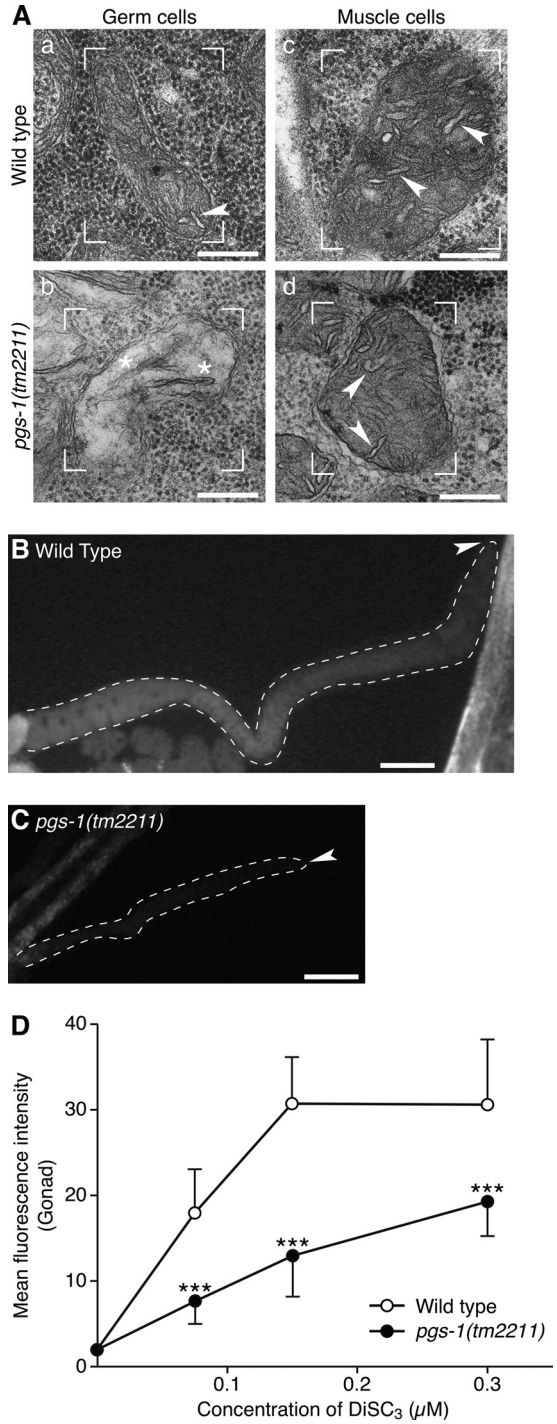

FIGURE 10. ***pgs-1* is required for the maintenance of mitochondrial morphology and function in germ cells.** *A*, mitochondrial cristae structures are disrupted in *pgs-1* germ cells. Transmission electron micrographs of germ cells (*panels a* and *b*) and muscle cells (*panels c* and *d*) in wild type and *pgs-1*(*tm2211*) are shown. In *pgs-1* germ cells, the mitochondria contained several elongated cristae structures in the mitochondrial matrix (*asterisk* in *panel c*). Representative mitochondria are enclosed by *brackets. Arrowheads* indicate the cristae structures. *Scale bars,* 200 nm. *B–D,* mitochondrial membrane potential is decreased in *pgs-1* germ cells. Representative fluorescence images of adult hermaphrodite germ cells in wild type (*B*) and *pgs-1*(*tm2211*) (*C*) stained with 0.15 μM $DiSC_3$ are shown. The gonads are outlined with the *dashed lines*. *Arrowheads* indicate the distal end of each gonad. *Scale bars,* 50 mm. *D,* quantification of the fluorescence intensity of $DiSC_3$ in germ cells of wild type and *pgs-1*(*tm2211*). The data represent the mean ± S.D. ***, $p < 0.001$.

distal end of the gonad proliferate by mitosis, and as they migrate proximally, they initiate meiosis at the transition zone (34). In *crls-1* mutants, the distal gonadal arm was reduced in size, and the number of oocytes was decreased (Fig. 2, *F* and *G*). DAPI staining revealed that the number of germ cells in the distal arm was reduced in *crls-1* mutants (Fig. 3, *A–C*). The reduced germ cell number was not due to enhanced apoptosis of germ cells because a mutation in *ced-3*, an essential gene for apoptotic cell death, did not restore normal germ cell number in *crls-1* mutants (data not shown). Although the number of germ cells was decreased, meiosis appeared to occur normally in *crls-1* mutants, *i.e. crls-1* mutant gonads contained crescent-shaped nuclei (leptotene/zygotene stage) in the transition zone, thread-like chromosomes (pachytene stage) in the meiotic zone, and highly condensed chromosomes (diakinesis stage) in the oocytes in a manner similar to those in wild type gonads (Fig. 3*D*). The reduced brood size of *crls-1* mutants was rescued by expression of *crls-1* under the control of a heat shock promoter, whereas expression of a catalytically inactive mutant *crls-1* (*crls-1*^{D116A}) failed to rescue the defect in *crls-1* mutants (Fig. 3*E*) (20, 32). Thus, *crls-1* is required for reproductive function through its enzymatic activity.

We further examined the mitotic capacity of germ cells by measuring the frequency of germ cell divisions, because division frequency often correlates with germ cell number (Fig. 4) (35, 36). In wild type gonads, more than 200 germ cells were present at the distal mitotic zone, and 2% of these germ cells had dividing nuclei as reported previously (Fig. 4, *A* and *C–E*) (27, 37). In contrast, the mitotic zone of the *crls-1* mutant gonads contained fewer germ cells, and dividing germ cells were found at lower frequency (Fig. 4, *B–E*). These data indicate that *crls-1* is required for the mitotic proliferation of germ cells in *C. elegans*.

Somatic Cell Proliferation Occurs Normally in crls-1 Mutants—Next, we examined somatic cell proliferation in *crls-1* mutants. In *C. elegans*, 556 somatic cells are generated from one fertilized egg during embryogenesis (38). A time-sequential observation revealed that somatic cells, such as intestinal cells and epithelial cells, proliferated and differentiated normally through somatic cell divisions in *crls-1* mutant embryos (data not shown). Consistent with this observation, *crls-1* mutants did not show any embryonic lethality (Table 1).

During the post-embryonic development of *C. elegans*, certain types of somatic cells, such as vulval cells and seam cells, proliferate to form somatic organs (the egg-laying apparatus and lateral epithelia, respectively) (38). During vulval development, three vulval precursor cells divide to produce 22 somatic vulval cells, forming the vulva at the adult stage (Table 2; Fig. 5*A*). In *crls-1* mutants, 22 vulval cells were presented in the normal configuration, and the morphology of the mature vulva was indistinguishable from that of the wild type, indicating that vulval cell divisions are not affected in *crls-1* mutants (Fig. 5, *B* and *C*). In addition to the vulval cells, seam cell divisions also occurred normally in *crls-1* mutants, *i.e.* all seam cells divided along the anterior-posterior axis to produce two daughter cells in a manner similar to that in the wild type (Fig. 6). Consistent

TABLE 3
Germ cell-enriched genes encoding putative mitochondrial proteins

Sequence name	Gene name	Predicted protein localization[a,b]	Brief description	Ref.
F28F8.2	*acs-2*	Mito, Ex	Long chain fatty acid acyl-CoA ligase	60
T05F1.2		Mito, Ex	Unnamed protein	
T22F3.4	*rpl-11.1*	Mito, Ex	Large ribosomal subunit L11 protein	
R09E10.6		Mito, Cyto	Unnamed protein	
F26H9.4		Mito, Cyto	Nicotinamide mononucleotide adenylyltransferase	
W01A11.7		Mito, Nuc	Unnamed protein	
F10D11.1	*sod-2*	Mito, Cyto	Manganese superoxide dismutase	61
T24D1.3		Mito, Nuc	Unnamed protein	
K08F4.11	*gst-3*	Mito, Cyto, Nuc	Glutathione *S*-transferase	
F35G12.10	*asb-1*	Mito, Pero, Ex	Mitochondrial F_1F_0-ATP synthase b subunit	52
T24C4.1	*ucr-2.3*	Mito, Nuc, Ex	Ubiquinol cytochrome *c* reductase complex core protein 2	
T16H12.5	*bath-43*	Mito, Cyto, Nuc	Speckle-type POZ protein SPOP and related proteins	
F45E4.9	*hmg-5*	Mito, Cyto, Nuc	HMG box-containing protein	62
C49C3.7		Mito, Cyto, Nuc	Unnamed protein	
T26A5.2		Mito, Nuc, Cyto, Ex	Unnamed protein	
K04C2.3		Mito, Cyto, Nuc, Ex	Unnamed protein	

[a] Protein localization was examined by WoLF PSORT, a computer program for the prediction of subcellular localization sites of proteins based on their amino acid sequences.
[b] The abbreviations used are as follows: Mito, mitochondria; Nuc, nucleus; Cyto, cytosol; Ex, extracellular.

with this, the seam cell number at the adult stage was the same as in the wild type (Table 2). Taken together, these data indicate that the somatic cell proliferation occurs normally throughout development in *crls-1* mutants.

crls-1 Is Required for the Maintenance of Mitochondrial Function and Morphology in Germ Cells but Not in Muscle Cells—Previous studies using yeast CL synthase mutants showed that a lack of CL causes a reduction in mitochondrial membrane potential (14–16, 18, 19, 39). Thus, we first stained *crls-1* mutants with $DiSC_3$, a membrane potentially sensitive mitochondrial dye (40), to evaluate the function of the mitochondria. The level of $DiSC_3$ fluorescence intensity indicated a significant reduction in mitochondrial membrane potential in *crls-1* germ cells (Fig. 7, *A* and *B*). However, $DiSC_3$ staining was not significantly affected in *crls-1* muscle cells (Fig. 7, *A* and *C*). Consistent with this observation, muscle function appeared normal in *crls-1* mutants as judged by the thrashing body movement in water (123.17 cycles/min in wild type *versus* 113.09 cycles/min in *crls-1* mutants).

We next examined the ultrastructural morphology of mitochondria in *crls-1* mutants by transmission electron microscopy (Fig. 8). In wild type germ cells, the mitochondria displayed many typical cristae that randomly crossed the mitochondrial matrix (*arrowheads* in Fig. 8*A*). However, in *crls-1* germ cells, cristae were not observed in the mitochondrial matrix, and elongated inner membranes were located along the edge of the mitochondria (*asterisk* in Fig. 8*B*). In contrast to the germ cells, mitochondrial morphology appeared normal in muscle cells in *crls-1* mutants (*arrowheads* in Fig. 8, *C* and *D*). These data indicate that *C. elegans crls-1* is required for the maintenance of mitochondrial function and morphology in germ cells but not in muscle cells.

Accumulation of PG Content Is Not Responsible for the Germ Cells Defects in crls-1 Mutants—To rule out the possibility that accumulation of PG causes the germ cell defects in *crls-1* mutants, we examined the phenotypes of *pgs-1*(*tm2211*), a deletion mutant lacking the phosphatidylglycerophosphate synthase gene (Fig. 9*A*). PGP synthase catalyzes the formation of PGP, a precursor of PG and CL, using CDP-DAG and glycerol 3-phosphate as substrates (Figs. 1*A* and 9*B*) (41, 42). Thus, lack of PGP synthase results in depletion of both PG and CL. In *pgs-1* mutants, germ cell divisions occurred infrequently, and the number of germ cells was decreased (Fig. 9, *C–I*) in a manner similar to *crls-1* mutants. In addition, deficiency of *pgs-1* caused the appearance of several elongated cristae structures in the mitochondrial matrix (Fig. 10*A*, *panels a* and *b*), and reduced mitochondrial membrane potential in germ cells (Fig. 10, *B–D*). In contrast, *pgs-1* mutants did not show obvious defects in somatic tissues, as judged by the divisions of vulval cells and seam cells (Table 2; Figs. 5 and 6), and mitochondrial morphology in muscle cells (Fig. 10*A*, *panels c* and *d*). These data indicate that loss of CL, but not accumulation of PG, causes the germ cell defects in *crls-1* mutants.

DISCUSSION

Previous studies using yeast showed that inhibition of CL synthase results in the instability of electron transport chain supercomplexes, a reduction in mitochondrial membrane potential, and a decrease in the oxidative phosphorylation rate (14, 16, 18, 19, 39, 43). In this study, by analyzing deletion mutants of the CL synthase gene (*crls-1*) in the simple multicellular organism *C. elegans,* we demonstrated that CL depletion selectively affects mitochondrial function and morphology in germ cells (Figs. 7 and 8). Furthermore, we found that CL is required for mitotic proliferation of germ cells but not that of somatic cells (Table 2; Figs. 4–6).

It is interesting that germ cells are more susceptible to CL depletion than somatic cells. Previous studies have indicated the mitochondrial heterogeneity in cell types with respect to morphological diversity (44, 45), steroidogenic capacity (46), protein profiles (47, 48), and lipid profiles (49, 50). Based on the existence of such mitochondrial heterogeneity, we propose two models that could explain the hypersensitivity of the germ cells to CL depletion. One possibility is that *in vivo*, CL is selectively required for germ cell-specific mitochondrial proteins. Using the genome-wide microarray data base generated by Reinke *et al.* (51), we found several germ cell-enriched genes encoding putative mitochondrial proteins, such as *asb-1*, *ucr-2.3*, *bath-43*, and *hmg-5* (Table 3). At this time, *in vivo* functions of most of these genes are largely unknown; however, *asb-1*, which

encodes a germ cell-specific isoform of mitochondrial ATP synthase b subunit, has been reported to be required for germ line development in *C. elegans* (52). CL may be needed to maintain the function and/or stability of such a germ cell-specific mitochondrial protein. The other possibility is that physical properties of the CL-depleted membrane vary between germ cells and somatic cells because of the difference in the mitochondrial lipid composition between these cell types (49, 50). In somatic cells such as muscle cells, mitochondrial lipids may compensate for a CL-depleted membrane environment by creating suitable microdomains for mitochondrial proteins, and thus, mitochondrial function and morphology are maintained in somatic cells. Recently, *Drosophila* mutants of a CL synthase gene were reported to exhibit abnormal mitochondrial morphology and function in muscle cells (53). The difference in the mitochondrial phenotype of muscle cells between *C. elegans* and *Drosophila melanogaster* may also be caused by the difference in the mitochondrial lipid composition between these species. For example, *D. melanogaster* lacks long chain polyunsaturated fatty acids that confer membrane fluidity (54).

In eukaryotes, cell division is regulated by cyclin and cyclin-dependent kinase. Inhibition of these general cell cycle regulators, such as *C. elegans* cyclin E (*cye-1*) and cyclin-dependent kinase-1 (*cdk-1*), reduces cell division of both germ cells and somatic cells, including the vulval cells and seam cells (55, 56), and thus, it causes lethality at a high frequency. In contrast, *crls-1* mutants grow to adulthood and exhibit defects in cell division specifically in germ cells (Table 1; Fig. 4). We found no defects in the cell division of somatic cells (Table 2; Figs. 5 and 6). These observations indicate that CL is not involved in the general cell division machinery. In *C. elegans,* germ cells are significantly more proliferative than somatic cells (34), which make the germ line a highly energy-consuming organ. It would appear that in *crls-1* mutants, the decrease in mitochondrial membrane potential in germ cells causes reduced energy production, which leads to inhibition of germ cell division. In the germ line of *C. elegans* hermaphrodite, sperm are produced during the late larval stage, and thereafter, oocytes are produced at the adult stage. Because the sperm and oocytes are produced from a common pool of progenitor germ cells, we assume that the reduced germ cell division of *crls-1* mutants affects not only oocyte production but also sperm production. This would lead to the striking reduction of brood size in *crls-1* mutants, the reduction occurring to a greater extent than would be expected from the reduction in germ cell division (Table 1; Fig. 4). To support this idea, crosses of *crls-1* mutant males to wild type hermaphrodites resulted in smaller brood sizes than those using wild type males and hermaphrodites (474.00 broods by wild type male *versus* 159.75 broods by *crls-1* mutant male).

This study demonstrates for the first time that the contribution of CL to mitochondrial function and morphology varies among the different cell types *in vivo*, raising the question of its generality. As mentioned above, *Drosophila* mutants of a CL synthase gene show abnormal mitochondrial morphology and function in muscle cells (53). In addition, disturbance of the CL remodeling causes abnormal mitochondrial morphology and function in muscle cells, such as the human Barth syndrome and the calcium-independent phospholipase $A_2\gamma$ knock-out mice (57, 58). To address this question, generation of CL synthase knock-out mice and subsequent analysis of their susceptibility to CL depletion in various tissues need to be carried out. In addition, *crls-1* mutants still contained residual CL, although *crls-1* is the single homologue of CL synthase in *C. elegans* (Fig. 2*C*). These data suggest that *C. elegans* has a bypass mechanism to produce CL except for the *de novo* synthetic pathway. Nonetheless, our study suggests the existence of a complementary system of the biomembrane in some cell types, at least in *C. elegans*. Further genetic analysis using *crls-1* mutants may reveal the molecular mechanisms underlying the different sensitivities of organelles to the changes in the lipid environment.

Acknowledgments—We greatly thank A. Takimoto and M. Ikuta for excellent technical assistance; Drs. K. Gengyo-Ando (Saitama University) and S. Mitani (Tokyo Women's Medical University School of Medicine) for providing alleles of crls-1 and pgs-1; Dr. A. Fire (Stanford University School of Medicine) for convenient vectors; and Dr. T. Inoue (National University of Singapore) for helpful discussions and comments on this study. Some strains were provided by the Caenorhabditis Genetics Center (University of Minnesota, Minneapolis), which is funded by the National Institutes of Health, NCRR.

REFERENCES

1. Schlame, M., Rua, D., and Greenberg, M. L. (2000) The biosynthesis and functional role of cardiolipin. *Prog. Lipid Res.* **39,** 257–288
2. Houtkooper, R. H., and Vaz, F. M. (2008) Cardiolipin, the heart of mitochondrial metabolism. *Cell. Mol. Life Sci.* **65,** 2493–2506
3. Joshi, A. S., Zhou, J., Gohil, V. M., Chen, S., and Greenberg, M. L. (2009) Cellular functions of cardiolipin in yeast. *Biochim. Biophys. Acta* **1793,** 212–218
4. Schlame, M., and Haldar, D. (1993) Cardiolipin is synthesized on the matrix side of the inner membrane in rat liver mitochondria. *J. Biol. Chem.* **268,** 74–79
5. Osman, C., Voelker, D. R., and Langer, T. (2011) Making heads or tails of phospholipids in mitochondria. *J. Cell Biol.* **192,** 7–16
6. Fry, M., and Green, D. E. (1981) Cardiolipin requirement for electron transfer in complex I and III of the mitochondrial respiratory chain. *J. Biol. Chem.* **256,** 1874–1880
7. Yu, C. A., and Yu, L. (1980) Structural role of phospholipids in ubiquinol-cytochrome *c* reductase. *Biochemistry* **19,** 5715–5720
8. Hayer-Hartl, M., Schägger, H., von Jagow, G., and Beyer, K. (1992) Interactions of phospholipids with the mitochondrial cytochrome *c* reductase studied by spin-label ESR and NMR spectroscopy. *Eur. J. Biochem.* **209,** 423–430
9. Schägger, H., Hagen, T., Roth, B., Brandt, U., Link, T. A., and von Jagow, G. (1990) Phospholipid specificity of bovine heart bc_1 complex. *Eur. J. Biochem.* **190,** 123–130
10. Gomez, B., Jr., and Robinson, N. C. (1999) Phospholipase digestion of bound cardiolipin reversibly inactivates bovine cytochrome bc_1. *Biochemistry* **38,** 9031–9038
11. Robinson, N. C., Zborowski, J., and Talbert, L. H. (1990) Cardiolipin-depleted bovine heart cytochrome *c* oxidase. Binding stoichiometry and affinity for cardiolipin derivatives. *Biochemistry* **29,** 8962–8969
12. Sedlák, E., and Robinson, N. C. (1999) Phospholipase A(2) digestion of cardiolipin bound to bovine cytochrome *c* oxidase alters both activity and quaternary structure. *Biochemistry* **38,** 14966–14972
13. Eble, K. S., Coleman, W. B., Hantgan, R. R., and Cunningham, C. C. (1990) Tightly associated cardiolipin in the bovine heart mitochondrial ATP synthase as analyzed by ^{31}P nuclear magnetic resonance spectroscopy. *J. Biol. Chem.* **265,** 19434–19440
14. Jiang, F., Ryan, M. T., Schlame, M., Zhao, M., Gu, Z., Klingenberg, M., Pfanner, N., and Greenberg, M. L. (2000) Absence of cardiolipin in the

crd1 null mutant results in decreased mitochondrial membrane potential and reduced mitochondrial function. *J. Biol. Chem.* **275,** 22387–22394
15. Koshkin, V., and Greenberg, M. L. (2000) Oxidative phosphorylation in cardiolipin-lacking yeast mitochondria. *Biochem. J.* **347,** 687–691
16. Koshkin, V., and Greenberg, M. L. (2002) Cardiolipin prevents rate-dependent uncoupling and provides osmotic stability in yeast mitochondria. *Biochem. J.* **364,** 317–322
17. Zhang, M., Mileykovskaya, E., and Dowhan, W. (2002) Gluing the respiratory chain together. Cardiolipin is required for supercomplex formation in the inner mitochondrial membrane. *J. Biol. Chem.* **277,** 43553–43556
18. Pfeiffer, K., Gohil, V., Stuart, R. A., Hunte, C., Brandt, U., Greenberg, M. L., and Schägger, H. (2003) Cardiolipin stabilizes respiratory chain supercomplexes. *J. Biol. Chem.* **278,** 52873–52880
19. Zhang, M., Mileykovskaya, E., and Dowhan, W. (2005) Cardiolipin is essential for organization of complexes III and IV into a supercomplex in intact yeast mitochondria. *J. Biol. Chem.* **280,** 29403–29408
20. Choi, S. Y., Gonzalvez, F., Jenkins, G. M., Slomianny, C., Chretien, D., Arnoult, D., Petit, P. X., and Frohman, M. A. (2007) Cardiolipin deficiency releases cytochrome *c* from the inner mitochondrial membrane and accelerates stimuli-elicited apoptosis. *Cell Death Differ.* **14,** 597–606
21. Huang, Z., Jiang, J., Tyurin, V. A., Zhao, Q., Mnuskin, A., Ren, J., Belikova, N. A., Feng, W., Kurnikov, I. V., and Kagan, V. E. (2008) Cardiolipin deficiency leads to decreased cardiolipin peroxidation and increased resistance of cells to apoptosis. *Free Radic. Biol. Med.* **44,** 1935–1944
22. Nomura, K., Imai, H., Koumura, T., Kobayashi, T., and Nakagawa, Y. (2000) Mitochondrial phospholipid hydroperoxide glutathione peroxidase inhibits the release of cytochrome *c* from mitochondria by suppressing the peroxidation of cardiolipin in hypoglycaemia-induced apoptosis. *Biochem. J.* **351,** 183–193
23. Lutter, M., Fang, M., Luo, X., Nishijima, M., Xie, X., and Wang, X. (2000) Cardiolipin provides specificity for targeting of tBid to mitochondria. *Nat. Cell Biol.* **2,** 754–761
24. Gonzalvez, F., and Gottlieb, E. (2007) Cardiolipin. Setting the beat of apoptosis. *Apoptosis* **12,** 877–885
25. Brenner, S. (1974) The genetics of *Caenorhabditis elegans*. *Genetics* **77,** 71–94
26. Gengyo-Ando, K., and Mitani, S. (2000) Characterization of mutations induced by ethyl methanesulfonate, UV, and trimethylpsoralen in the nematode *Caenorhabditis elegans*. *Biochem. Biophys. Res. Commun.* **269,** 64–69
27. Maciejowski, J., Ugel, N., Mishra, B., Isopi, M., and Hubbard, E. J. (2006) Quantitative analysis of germ line mitosis in adult *C. elegans*. *Dev. Biol.* **292,** 142–151
28. Timmons, L. (2004) Endogenous inhibitors of RNA interference in *Caenorhabditis elegans*. *BioEssays* **26,** 715–718
29. Simmer, F., Tijsterman, M., Parrish, S., Koushika, S. P., Nonet, M. L., Fire, A., Ahringer, J., and Plasterk, R. H. (2002) Loss of the putative RNA-directed RNA polymerase RRF-3 makes *C. elegans* hypersensitive to RNAi. *Curr. Biol.* **12,** 1317–1319
30. Bligh, E. G., and Dyer, W. J. (1959) A rapid method of total lipid extraction and purification. *Can. J. Biochem. Physiol.* **37,** 911–917
31. Rouser, G., Fkeischer, S., and Yamamoto, A. (1970) Two-dimensional thin layer chromatographic separation of polar lipids and determination of phospholipids by phosphorus analysis of spots. *Lipids* **5,** 494–496
32. Williams, J. G., and McMaster, C. R. (1998) Scanning alanine mutagenesis of the CDP-alcohol phosphotransferase motif of *Saccharomyces cerevisiae* cholinephosphotransferase. *J. Biol. Chem.* **273,** 13482–13487
33. Jiang, F., Rizavi, H. S., and Greenberg, M. L. (1997) Cardiolipin is not essential for the growth of *Saccharomyces cerevisiae* on fermentable or nonfermentable carbon sources. *Mol. Microbiol.* **26,** 481–491
34. Kimble, J., and Hirsh, D. (1979) The postembryonic cell lineages of the hermaphrodite and male gonads in *Caenorhabditis elegans*. *Dev. Biol.* **70,** 396–417
35. Ariz, M., Mainpal, R., and Subramaniam, K. (2009) *C. elegans* RNA-binding proteins PUF-8 and MEX-3 function redundantly to promote germ line stem cell mitosis. *Dev. Biol.* **326,** 295–304
36. Michaelson, D., Korta, D. Z., Capua, Y., and Hubbard, E. J. (2010) Insulin signaling promotes germ line proliferation in *C. elegans*. *Development* **137,** 671–680
37. Crittenden, S. L., Leonhard, K. A., Byrd, D. T., and Kimble, J. (2006) Cellular analyses of the mitotic region in the *Caenorhabditis elegans* adult germ line. *Mol. Biol. Cell* **17,** 3051–3061
38. Sulston, J. E., and Horvitz, H. R. (1977) Post-embryonic cell lineages of the nematode, *Caenorhabditis elegans*. *Dev. Biol.* **56,** 110–156
39. Zhang, M., Su, X., Mileykovskaya, E., Amoscato, A. A., and Dowhan, W. (2003) Cardiolipin is not required to maintain mitochondrial DNA stability or cell viability for *Saccharomyces cerevisiae* grown at elevated temperatures. *J. Biol. Chem.* **278,** 35204–35210
40. Gásková, D., DeCorby, A., and Lemire, B. D. (2007) DiS-C3(3) monitoring of *in vivo* mitochondrial membrane potential in *C. elegans*. *Biochem. Biophys. Res. Commun.* **354,** 814–819
41. Chang, S. C., Heacock, P. N., Clancey, C. J., and Dowhan, W. (1998) The *PEL1* gene (renamed PGS1) encodes the phosphatidylglycero-phosphate synthase of *Saccharomyces cerevisiae*. *J. Biol. Chem.* **273,** 9829–9836
42. Kawasaki, K., Kuge, O., Chang, S. C., Heacock, P. N., Rho, M., Suzuki, K., Nishijima, M., and Dowhan, W. (1999) Isolation of a Chinese hamster ovary (CHO) cDNA encoding phosphatidylglycerophosphate (PGP) synthase, expression of which corrects the mitochondrial abnormalities of a PGP synthase-defective mutant of CHO-K1 cells. *J. Biol. Chem.* **274,** 1828–1834
43. Zhong, Q., Gohil, V. M., Ma, L., and Greenberg, M. L. (2004) Absence of cardiolipin results in temperature sensitivity, respiratory defects, and mitochondrial DNA instability independent of pet56. *J. Biol. Chem.* **279,** 32294–32300
44. Munn, E. A. (1974) *The Structure of Mitochondria,* pp. 1–69, Academic Press, New York
45. Kuznetsov, A. V., Hermann, M., Saks, V., Hengster, P., and Margreiter, R. (2009) The cell type specificity of mitochondrial dynamics. *Int. J. Biochem. Cell Biol.* **41,** 1928–1939
46. Hanukoglu, I. (1992) Steroidogenic enzymes. Structure, function, and role in regulation of steroid hormone biosynthesis. *J. Steroid Biochem. Mol. Biol.* **43,** 779–804
47. Mootha, V. K., Bunkenborg, J., Olsen, J. V., Hjerrild, M., Wisniewski, J. R., Stahl, E., Bolouri, M. S., Ray, H. N., Sihag, S., Kamal, M., Patterson, N., Lander, E. S., and Mann, M. (2003) Integrated analysis of protein composition, tissue diversity, and gene regulation in mouse mitochondria. *Cell* **115,** 629–640
48. Johnson, D. T., Harris, R. A., French, S., Blair, P. V., You, J., Bemis, K. G., Wang, M., and Balaban, R. S. (2007) Tissue heterogeneity of the mammalian mitochondrial proteome. *Am. J. Physiol. Cell. Physiol.* **292,** C689–C697
49. Courtade, S., Marinetti, G. V., and Stotz, E. (1967) The structure and abundance of rat tissue cardiolipins. *Biochim. Biophys. Acta* **137,** 121–134
50. White, D. A. (1973) in *Form and Function of Phospholipids* (Ansell G. B., Hawthorne J. N., and Dawson R. M. C., eds) pp. 441–482, Elsevier Scientific Publishing Co., Inc., New York
51. Reinke, V., Smith, H. E., Nance, J., Wang, J., Van Doren, C., Begley, R., Jones, S. J., Davis, E. B., Scherer, S., Ward, S., Kim, S. K. (2000) A global profile of germ line gene expression in *C. elegans*. *Mol. Cell* **6,** 605–616
52. Kawasaki, I., Hanazawa, M., Gengyo-Ando, K., Mitani, S., Maruyama, I., and Iino, Y. (2007) ASB-1, a germ line-specific isoform of mitochondrial ATP synthase *b* subunit, is required to maintain the rate of germ line development in *Caenorhabditis elegans*. *Mech. Dev.* **124,** 237–251
53. Acehan, D., Malhotra, A., Xu, Y., Ren, M., Stokes, D. L., and Schlame, M. (2011) Cardiolipin affects the supramolecular organization of ATP synthase in mitochondria. *Biophys. J.* **100,** 2184–2192
54. Shen, L. R., Lai, C. Q., Feng, X., Parnell, L. D., Wan, J. B., Wang, J. D., Li, D., Ordovas, J. M., and Kang, J. X. (2010) *Drosophila* lacks C20 and C22 PUFAs. *J. Lipid Res.* **51,** 2985–2992
55. Boxem, M., Srinivasan, D. G., and van den Heuvel, S. (1999) The *Caenorhabditis elegans* gene *ncc-1* encodes a cdc2-related kinase required for M phase in meiotic and mitotic cell divisions, but not for S phase. *Development* **126,** 2227–2239
56. Fay, D. S., and Han, M. (2000) Mutations in cye-1, a *Caenorhabditis elegans* cyclin E homolog, reveal coordination between cell cycle control and vulval development. *Development* **127,** 4049–4060

57. Acehan, D., Vaz, F., Houtkooper, R. H., James, J., Moore, V., Tokunaga, C., Kulik, W., Wansapura, J., Toth, M. J., Strauss, A., and Khuchua, Z. (2011) Cardiac and skeletal muscle defects in a mouse model of human Barth syndrome. *J. Biol. Chem.* **286,** 899–908
58. Mancuso, D. J., Sims, H. F., Han, X., Jenkins, C. M., Guan, S. P., Yang, K., Moon, S. H., Pietka, T., Abumrad, N. A., Schlesinger, P. H., and Gross, R. W. (2007) Genetic ablation of calcium-independent phospholipase $A_2\gamma$ leads to alterations in mitochondrial lipid metabolism and function resulting in a deficient mitochondrial bioenergetic phenotype. *J. Biol. Chem.* **282,** 34611–34622
59. Mello, C. C., Kramer, J. M., Stinchcomb, D., and Ambros, V. (1991) Efficient gene transfer in *C. elegans.* Extrachromosomal maintenance and integration of transforming sequences. *EMBO J.* **10,** 3959–3970
60. Van Gilst, M. R., Hadjivassiliou, H., and Yamamoto, K. R. (2005) A *Caenorhabditis elegans* nutrient response system partially dependent on nuclear receptor NHR-49. *Proc. Natl. Acad. Sci. U.S.A.* **102,** 13496–13501
61. Hunter, T., Bannister, W. H., and Hunter, G. J. (1997) Cloning, expression, and characterization of two manganese superoxide dismutases from *Caenorhabditis elegans. J. Biol. Chem.* **272,** 28652–28659
62. Sumitani, M., Kasashima, K., Matsugi, J., and Endo, H. (2011) Biochemical properties of *Caenorhabditis elegans* HMG-5, a regulator of mitochondrial DNA. *J. Biochem.* **149,** 581–589